Experimental Eye Research 264 (2026) 110861

Contents lists available at ScienceDirect

Experimental Eye Research

journal homepage: www.elsevier.com/locate/yexer

Research article

Rapid anterior segment and divergent corneal shape remodeling drive astigmatic compensation in the chick model

Yuanyuan Liang [a,*], Tsz Wing Leung [a,b,c], Patience Ansomah Ayerakwah [a], Byung Soo Kang [a], Chea-su Kee [a,b,c,**]

[a] School of Optometry, The Hong Kong Polytechnic University, Hong Kong, China
[b] Research Centre for SHARP Vision (RCSV), The Hong Kong Polytechnic University, Hong Kong, China
[c] Centre for Eye and Vision Research (CEVR), 17W Hong Kong Science Park, Hong Kong, China

ARTICLE INFO

Keywords:
Astigmatism
Cornea
Crystalline lens
Anterior chamber depth
Chicken

ABSTRACT

This study investigated early temporal dynamics of ocular compensation to imposed astigmatic blur, specifically anterior segment alterations in a chick model. Fifty-four chickens were equally randomized to treatment or control groups at post-hatching day 5 (baseline, T0). Crossed-cylindrical lens (+4.00 DS/−8.00 DC) was used to induce astigmatic blur on the right eye for two weeks: With-the-rule (WTR, axis 90°) and Against-the-rule (ATR, axis 180°) astigmatism. Ocular axial dimensions and objective refraction were measured daily for the first four days (T0-T3), and at one (T7) and two weeks (T14). Corneal topography was measured at T3, T7 and T14. Our results showed that chicks treated with crossed-cylindrical lenses developed significantly higher refractive astigmatism compared to the control group (all $p < 0.01$), plateauing within two days. Corneal astigmatism diverged over two weeks, increasing in the WTR group but decreasing in the ATR groups, while internal astigmatism showed opposite trends. Critically, anterior segment changes emerged by T3: the ATR group exhibited a significantly deeper anterior chamber (T3: $p = 0.034$), and both treatment groups showed significantly thinner crystalline lenses (ATR: T2, $p = 0.008$; T3, $p = 0.007$; WTR: T3, $p = 0.043$) compared to controls. These changes persisted throughout the treatment. To conclude, refractive astigmatism compensated rapidly (plateauing within two days) in response to astigmatic blur, while corneal astigmatism exhibited divergent changes over two weeks. The persistent anterior segment alterations—lens thinning and anterior chamber deepening—demonstrate a key compensatory role for anterior ocular structures beyond corneal plasticity alone.

1. Introduction

Regular astigmatism (cylindrical error [Cyl] > 0.5 D) is a prevalent refractive error in which the eye has two orthogonal principal meridians, causing light to focus as two perpendicular line foci rather than a single point. It primarily arises from toricity in the cornea or crystalline lens, affecting 14.9 % of schoolchildren and 40.4 % of adults globally (Hashemi et al., 2018). Uncorrected astigmatism degrades vision at all distances and can cause permanent meridional visual deficits if left untreated during the critical period of visual development (Zhang et al., 2022; Leung et al., 2021; Wang et al., 2018; Mitchell et al., 1973). Unlike myopia – which typically stabilizes in adulthood (COMET-Group, 2013; Qin et al., 2022) – astigmatism exhibits dynamic shifts in both magnitude and axis throughout life (Kee, 2013; Read et al., 2007). Consequently, it significantly impairs quality of life and may be associated with myopia progression (Kearney et al., 2025), hindering night driving (Black et al., 2019) and reducing overall well-being (Wolffsohn et al., 2011), thereby imposing substantial societal burdens (Zhang et al., 2023).

It is well-established that visual signals guide eye growth through short-term choroidal adjustments and long-term scleral remodeling (Wallman and Winawer, 2004). For example, spherical defocus (i.e. hyperopic or myopic blur), which focuses an image in front of or behind the retina, could elicit the rapid response of the choroid by adjusting the position of the retina forward or backward to achieve emmetropia in response to imposed defocus (Wallman et al., 1995), and it occurs within a few minutes of exposure to defocus in the chick model (Zhu et al., 2005; Zhu and Wallman, 2009). Despite the quick action of choroid, it is

* Corresponding author. School of Optometry, The Hong Kong Polytechnic University, 11 Yuk Choi Road, Hung Hom, Kowloon, Hong Kong, China.
** Corresponding author. School of Optometry, The Hong Kong Polytechnic University, 11 Yuk Choi Road, Hung Hom, Kowloon, Hong Kong, China.
E-mail addresses: 22117026r@connect.polyu.hk (Y. Liang), c.kee@polyu.edu.hk (C.-s. Kee).

https://doi.org/10.1016/j.exer.2026.110861
Received 4 November 2025; Received in revised form 14 December 2025; Accepted 11 January 2026
Available online 13 January 2026

reported that the axial elongation exceeds that of the fellow eye after only one day of wearing a negative lens (−15 D) and three days for diffusers, mainly due to increased vitreous chamber depth, while anterior segment dimensions remain stable (i.e. anterior chamber dimension: distance between anterior cornea to anterior lens; and lens thickness) (Kee et al., 2001). In terms of change in the anterior segments (i.e., corneal curvature and anterior chamber depth), the results are inconsistent compared to the posterior segments. For example, a steeper cornea and an increased anterior chamber depth are observed in the form-deprived chick eye (Gottlieb et al., 1987; Kang et al., 2024; Troilo et al., 1995), while the anterior chamber depth is relatively stable under defocus exposure with normal light level (500 lux) or even with high level light intensity (15,000 lux) (Ashby and Schaeffel, 2010). Despite the rich evidence on the mechanisms of spherical refractive error development (Troilo et al., 2019), astigmatism remains understudied, particularly regarding the anterior segment in its development.

Although astigmatism primarily arises from anterior segments (i.e., cornea and crystalline lens), and our previous work demonstrated compensatory refractive changes in response to astigmatic defocus (Chu and Kee, 2015; Popa et al., 2020; Vyas and Kee, 2021; Ayerakwah et al., 2025), the temporal dynamics of astigmatism development remain unknown. In this study, we hypothesize that sustained astigmatic blur drives astigmatism progression in chicks through coordinated changes in corneal shape, crystalline lens thickness, and anterior chamber depth. Furthermore, we aim to investigate whether adaptation patterns differ between early (≤3 days) and sustained (1–2 weeks) exposure. Using the chick model − a well-established system for refractive development studies (Irving et al., 1991, 1995; Troilo et al., 2019) − we longitudinally assess corneal topography, refractive error, and ocular axial components during early (3-day) and long-term (1- and 2-week) astigmatic blur exposure. This hypothesis-driven approach will clarify how anterior segment parameters contribute to astigmatism development, bridging a critical gap for further mechanism investigation.

2. Methods

2.1. Animal model

Fifty-four White Leghorn chickens (*Gallus gallus domesticus*) were hatched from specific-pathogen-free eggs (Jinan SPAFAS Poultry Co., Jinan, China) and raised at The Hong Kong Polytechnic University's Centralized Animal Facility. The animal room maintained a 12h:12h Light:Dark cycle with 150 lux illumination at eye level from 7 a.m. to 7 p.m. Chickens had *ad libitum* access to food and water. All experiments adhered to the ARVO Statement for the Use of Animals in Ophthalmic and Vision Research, and the study protocol was approved by the Animal Subjects Ethics Subcommittee (ASESC 23–395) of The Hong Kong Polytechnic University.

2.2. Animal treatments

On post-hatching day 5 (P5), or treatment day 0 (T0), chickens were randomized into control (n = 18) and two treatment groups (n = 36). P5 was selected to minimize the potential confounding effects of natural astigmatism with lens-induced astigmatism on eye growth (Vyas and Kee, 2021). Astigmatic blur was optically imposed in the right eyes by attaching crossed-cylindrical lenses (+4.00 DS/-8.00 DC, PMMA material, base curve = 7.5 mm, diameter = 10.8 mm, optical zone = 10 mm; Conforma, VA, USA) oriented at 90° (With-The-Rule, WTR; n = 18) or 180° (Against-The-Rule, ATR; n = 18) for two weeks, with the axis of the lenses referenced to the canthi (Irving et al., 1995). To be specific, the orientation of optically induced astigmatism was determined by the axis setting of the treatment lens: With-the-rule (WTR) astigmatism was simulated by placing the minus-cylinder axis at 90°, so that the positive (+4.00 DC axis 180) and negative cylindrical powers (−4.00 DC axis 90) were positioned along the 90° and 180° powered meridians, respectively. The current power induces higher astigmatism than weaker alternatives used in the previous study (Chu and Kee, 2015). Lenses were affixed via a Velcro ring adhered peri-orbitally (Norland Products, New Brunswick, NJ, USA) and cleaned daily (<1 min) with cotton swabs.

2.3. Ocular biometric measurements

To minimize diurnal variations in ocular measurements (Nickla et al., 1998), all biometric measurements were conducted between 8 a.m. and 12 p.m. Corneal topography was first assessed using a custom-built Placido-based Videokeratography system (Chu et al., 2014). Refractive status was then determined with a modified Hartinger refractometer, recording three readings per eye (Kee and Deng, 2008). Finally, ocular axial dimensions were measured using a high-resolution A-scan ultrasonography (Kang et al., 2018).

2.3.1. Videokeratography system (VKS)

Corneal shape was measured in awake chickens with eyes naturally open using a Placido-ring VKS. After aligning the pupil with the rings, a CCD camera captured corneal reflections. At least three sharply focused images per eye were selected according to established criteria and analyzed using a custom MATLAB algorithm (Chu et al., 2014; Kang et al., 2024). Of the three tested zones (1.50, 2.10, and 2.80 mm diameter), we analyzed only the central 2.80 mm zone because it yielded the highest accuracy and lowest instrumental noise in sphere-based validation (maximum deviations: 1.50 mm vs 2.80 mm corneal astigmatism = −0.45 D vs −0.18 D; J0 = −0.02 D vs −0.01 D; J45 = −0.22 D vs −0.09 D) (Chu et al., 2014), and it aligns with prior chick studies (Chu et al., 2014; Ayerakwah et al., 2025) to support repeatability and comparability. Measurements were obtained at 3 days (T3), 1 week (T7), and 2 weeks (T14) post-treatment. Earlier measurements (T0-T2) were precluded by insufficient corneal size for reliable topography acquisition.

2.3.2. Hartinger coincidence refractometer

Refractive status was measured using a Hartinger coincidence refractometer (Model 110, Carl Zeiss Meditec, Germany). Chickens were anesthetized with isoflurane (0.75 %–1.0 % in oxygen), and the palpebral fissure was aligned horizontally. A custom eyelid retractor was used to gently open the eye during measurements (Kee and Deng, 2008). Three readings were recorded per eye. Refraction was performed daily during the first 4 days (T0-T3), and then at 1 week (T7) and 2 weeks (T14).

2.3.3. A-scan ultrasonography

Ocular axial dimensions were measured using a custom-built A-scan ultrasound system with a 50 MHz transducer coupled with an adjustable pulse-receiver (PVDF; PI50-2-R0.50; GE Panametrics, U.S.) Parameters include: central corneal thickness (CCT), anterior chamber depth (ACD), lens thickness (LT), vitreous chamber depth (VCD), retinal thickness (RT), choroidal thickness (ChT), scleral thickness (SL) and axial length (AXL; anterior cornea to posterior sclera). Under isoflurane anesthesia, eyes were gently opened with an eyelid retractor. The probe was aligned along the pupillary axis after applying ultrasound gel (New Jersey, USA) to its surface. To minimize the potential impact of gel on the cornea, a drop of distilled water was applied to the corneal surface to reduce irritation. Additionally, three measurements per eye were acquired within 2 min with measurement order randomized—alternating the starting eye between chicks. Data were analyzed using a custom peak-identification algorithm (Nickla et al., 1998) and averaged. Measurements occurred daily during the first 4 days (T0-T3), then at 1 week (T7) and 2 weeks (T14).

2.4. Data analysis

Data were analyzed using SPSS (version 22, IBM Corp., Armonk, NY, USA) with a significance level of $\alpha < 0.05$. Astigmatism was decomposed into J0 and J45 components using power vector analysis (Thibos et al., 1997), where positive J0 indicates WTR astigmatism, negative J0 indicates ATR astigmatism, and J45 indicates oblique astigmatism. Internal astigmatism (IA) was calculated as the vector difference between the refractive and corneal J0 and J45 astigmatic components. Finally, IA was converted into cylindrical power based on these vector components. To avoid potential confounding effects of astigmatic blur on the fellow untreated eye, only data of the treated (right) eyes were used for analysis. Subsequent analysis showed no significant difference among fellow eyes of treated and control groups. A repeated two-way ANOVA with Bonferroni's post-hoc test was used to compare changes in ocular parameters across groups, with time as the within-group factor and treatment as the between-group factor. Greenhouse-Geisser or Huynh-Feldt corrections were applied based on data sphericity from Mauchly's test. Pearson or Spearman correlation analysis was conducted between corneal and ocular components, depending on data normality. Results were expressed as mean ± standard deviation (SD) to depict the variability of individual measurements within each group and the dispersion between treated and control conditions.

3. Results

3.1. Development of refractive astigmatism

Significant treatment, time, and interaction effects were observed for refractive astigmatism (Treatment: $F_{(2, 51)} = 144.0$; Time: $F_{(3.51, 179.2)} = 31.35$; Interaction: $F_{(10, 26)} = 13.68$; all $p < 0.001$). Treatment groups developed significantly higher refractive astigmatism (RA) than controls, with profound effects during the early phase (Fig. 1A, T0 – T3). RA increased sharply in both treated groups in one day (vs. controls: $p < 0.01$), peaking after two days (WTR > ATR, $p = 0.02$; both vs. controls $p < 0.001$). RA stabilized post-treatment day 2 (plateau: $p \geq 0.18$), while controls remained stable (<0.5D, $p \geq 0.15$). The ANOVA-identified temporal pattern (rapid increase and plateau) was further quantified via piecewise growth modeling (see Supplementary Material).

For refractive-J0 (R-J0, Fig. 1B), treatment groups showed compensatory shifts (Treatment: $F_{(2,51)} = 210.9$, $p < 0.001$; Time: $F_{(3.80,194.0)} = 3.66$, $p = 0.008$; Interaction: $F_{(10,255)} = 24.34$, $p < 0.001$). WTR eyes developed strongly negative values ($p < 0.001$ vs. controls), increasing sharply over the first two days (all $p < 0.002$) before plateauing, mirroring RA dynamics. ATR eyes showed mild positive shifts ($p < 0.05$) but no temporal changes (high variability).

For R-J45 (Fig. 1C), significant treatment ($F_{(2,51)} = 23.20$, $p < 0.001$) and interaction effects ($F_{(10,255)} = 3.85$, $p < 0.001$) were observed, with no time effect ($F_{(2.94,149.7)} = 1.03$, $p = 0.38$). WTR surpassed controls at T1 ($p < 0.03$), diverging from ATR by T7 ($p < 0.001$). Controls remained stable (all $p \geq 0.05$).

3.2. Development of corneal astigmatism

Repeated ANOVA revealed strong treatment and interaction effects on CA (Treatment: $F_{(2,51)} = 28.93$, $p < 0.001$; Interaction: $F_{(4,102)} = 8.98$, $p < 0.001$), with both WTR and ATR groups exceeding controls ($p \leq 0.005$ by T3) (Fig. 2A). WTR's CA increased progressively (T14 > T3/T7, $p \leq 0.004$), while ATR's declined after T3 (T14 < T3, $p = 0.02$), diverging significantly by T14 (3.00D vs. 1.62D, $p < 0.001$). Controls remained stable (~1D, $p > 0.35$).

For corneal-J0 (C-J0), treatment ($F_{(2,51)} = 42.17$), time ($F_{(1.99,101.7)} = 51.99$), and interaction ($F_{(4,102)} = 13.02$) effects were significant (Fig. 2B, all $p < 0.001$). ATR shifted positively vs. WTR/controls (all $p < 0.001$), except T14 (vs. control: $p = 0.68$). WTR became progressively more negative ($p < 0.05$), mirroring R-J0 trends, while controls remained stable ($p > 0.52$). For corneal-J45 (C-J45), treated groups showed more negative values than controls ($F_{(2,51)} = 33.30$, $p < 0.001$) but no time ($p = 0.13$) or interaction effects ($p = 0.74$) (Fig. 2C).

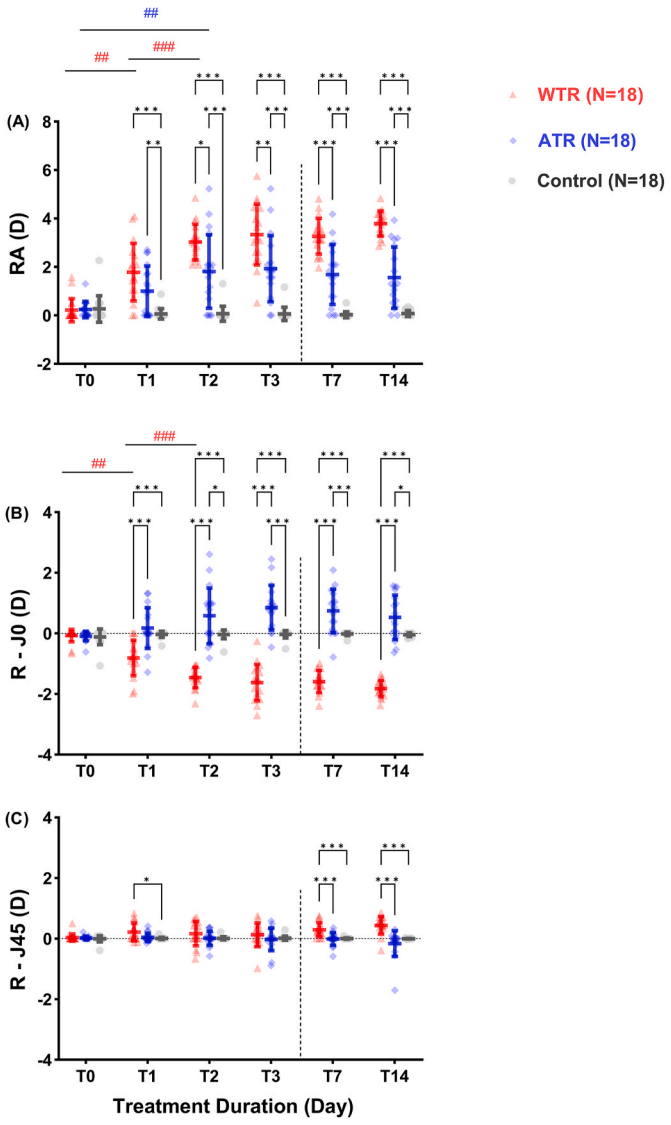

Fig. 1. Longitudinal changes in refractive astigmatism components in the treated and control eyes. The X axis represents treatment duration, and the Y axis is the refractive component: (A) Magnitude of refractive astigmatism (**RA**), (B) R-J0 astigmatic component (**R-J0),** and (C) R-J45 astigmatic component (**R-J45**). The vertical dashed line in the figures separates data into early and long-term phase exposure. Data shown as mean ± SD (dots: individual birds). Groups: WTR (red), ATR (blue), control (grey). Symbols: * (treatment effect), # (time effect); one/two/three symbols = p < 0.05/<0.01/<0.001. (For interpretation of the references to colour in this figure legend, the reader is referred to the Web version of this article.)

The flattest corneal meridian in treated groups became significantly flatter than controls by T7 (both $p < 0.05$), persisting in WTR at T14 ($p = 0.008$) (Fig. 2D). The steepest meridian showed time-dependent flattening ($F_{(1.96,100.1)} = 1419$, $p < 0.001$) but no treatment effects ($p \geq 0.15$).

3.3. Development of internal astigmatism

Repeated two-way ANOVA showed significant treatment, time, and interaction effects on IA (Treatment: $F_{(2, 51)} = 54.33$, $p < 0.001$; Time: $F_{(1.97, 100.6)} = 5.11$, $p = 0.008$; Interaction: $F_{(4, 102)} = 3.4$; $p = 0.01$). Both

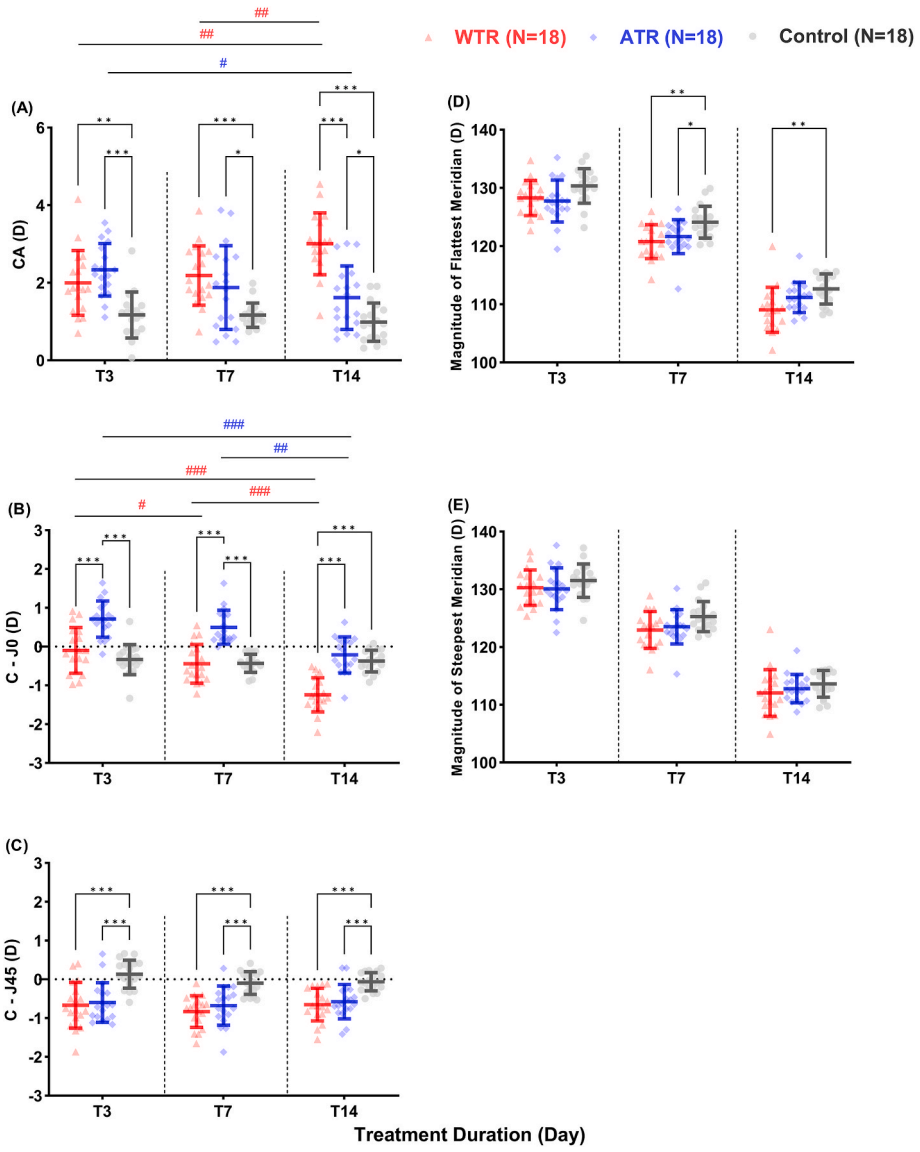

Fig. 2. Longitudinal changes in corneal astigmatism components in the treated and control groups. The X axis represents treatment duration, and the Y axis is the corneal component: (A) Magnitude of corneal astigmatism (**CA**), (B) C-J0 astigmatic component (**C-J0**), (C) C-J45 astigmatic component (**C-J45**), (D) magnitude of the flattest meridian, and (E) magnitude of the steepest meridian. Data: mean ± SD (dots: individual birds). Groups: WTR (red), ATR (blue), control (grey). Symbols: * (treatment effect), # (time effect); one/two/three symbols = p < 0.05/<0.01/<0.001. (For interpretation of the references to colour in this figure legend, the reader is referred to the Web version of this article.)

WTR and ATR groups showed higher magnitudes of IA than controls throughout the treatment period ($p \leq 0.002$) (Fig. 3A). WTR's IA decreased over time ($p \leq 0.04$), showing a trend opposite to that observed in corneal astigmatism (Fig. 2A), whereas IA in the ATR and control groups remained stable ($p > 0.23$).

For internal J0 (I-J0), treatment ($F_{(2,51)} = 81.6$, $p < 0.001$), time ($F_{(1.93,98.25)} = 13.3$, $p < 0.001$), and interaction ($F_{(4,102)} = 3.92$, $p = 0.005$) effects were significant (Fig. 3B, all $p \leq 0.005$). Both WTR and ATR shifted positively compared to controls (all $p \leq 0.037$), exhibiting a reversed trend compared to C-J0 (Fig. 2B), while controls remained stable ($p > 0.66$). For internal J45 (I-J45), significant treatment ($F_{(2,51)} = 52.04$, $p < 0.001$) and time effects ($F_{(1.59,\ 81.04)} = 2.70$, $p = 0.009$) were observed, but no interaction effects ($F_{(4,\ 102)} = 1.15$, $p = 0.34$). Both treated groups showed more positive values than controls ($p \leq 0.03$) (Fig. 3C). Time effect was not significant after adjustment for multiple comparisons within the group.

3.4. Effects on ocular axial components

As shown in Fig. 4, both ATR- and WTR-treated eyes exhibited progressive anterior chamber deepening (ACD: Treatment: $F_{(2,51)} = 8.86$, $p < 0.001$; Interaction: $F_{(10,255)} = 9.61$, $p < 0.001$), with ATR showing significantly deeper ACD than controls by T3 ($p = 0.04$) and surpassing WTR by T14 ($p < 0.001$). Lens thinning (LT: treatment: $F_{(2,51)} = 6.16$, $p = 0.004$) mirrored these trends: ATR reduced LT versus controls at T2/T3 ($p \leq 0.009$), while WTR thinned later (T7/T14, $p \leq 0.003$), aligning temporally with corneal steepest/flattest meridian shifts (Fig. 2D and E). These anterior changes–absent in controls ($p > 0.35$ for CA stability)—suggest cornea-lens interplay underlies compensatory astigmatism.

Posterior segment alterations were limited: WTR retinas thinned versus controls at T7/T14 ($p \leq 0.04$), with transient choroidal thickening at T1 ($p = 0.01$), but no sustained treatment effects (ChT: $p > 0.05$). No changes occurred in corneal thickness, vitreous chamber depth, scleral thickness, axial length, or fellow eyes (all $p > 0.05$), underscoring anterior dominance in astigmatism induction.

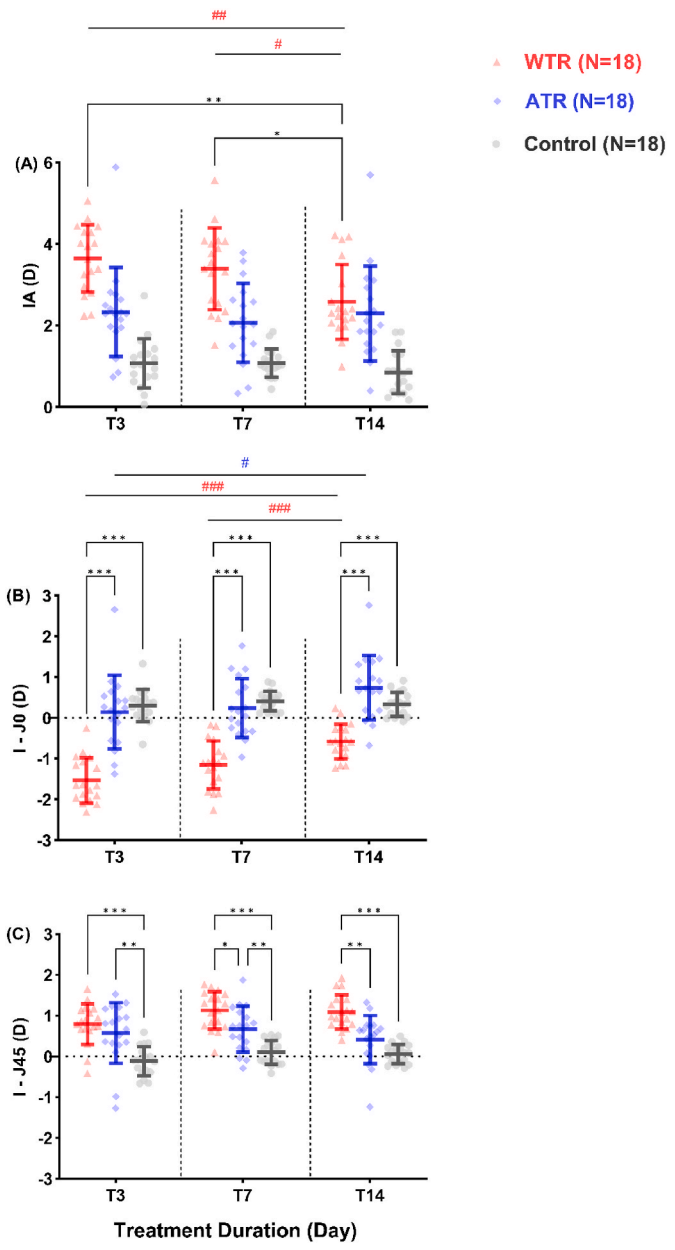

Fig. 3. Longitudinal changes in internal astigmatism components in treated and control group. The X axis represents treatment duration, and the Y axis is the internal astigmatic component: (A) Magnitude of internal astigmatism (**IA**), (B) I-J0 astigmatic component (**I-J0**), and (C) I-J45 astigmatic component (**I-J45**). Data: mean ± SD (dots: individual birds). Groups: WTR (red), ATR (blue), control (grey). Symbols: * (treatment effect), # (time effect); one/two/three symbols = p < 0.05/<0.01/<0.001. (For interpretation of the references to colour in this figure legend, the reader is referred to the Web version of this article.)

3.5. Correlation analysis

Since corneal astigmatism (CA) is defined as the difference in magnitude between the steepest and flattest principal meridians of the cornea, we used correlation analysis to assess how these meridians relate to ocular components. The results are presented in Table 1.

In the WTR group, ACD showed a negative correlation with the flattest meridian at T3 ($r = -0.61$, $p = 0.008$). VCD demonstrated moderate-to-high correlations with the flattest meridian at T3/T7/T14 ($r \leq 0.67$, $p \leq 0.002$). Both retinal and choroidal thickness were positively correlated with the flattest meridian at T14 ($r \geq 0.54$, $p \leq 0.022$). Comparable correlations were observed for the steepest meridian. After Bonferroni correction (adjusted $p = 0.0024$), only VCD correlations with both meridians remained significant ($p < 0.001$).

In the ATR group, CCT showed negative correlations with the flattest meridian at T7/T14 ($p \leq 0.035$), while VCD was negatively associated with the flattest meridian at T14 ($p = 0.029$). After Bonferroni correction (adjusted $p = 0.0024$), these correlations became non-significant. For the steepest meridian, only VCD maintained a significant negative correlation at T14 ($r = -0.67$, $p = 0.002$) after Bonferroni correction.

4. Discussion

The present study provides compelling evidence in a widely used animal model in astigmatism research, demonstrating that induced astigmatic blur exerts rapid, direction-dependent effects on refractive development, with critical anterior segment alterations emerging as a central compensatory mechanism. Our findings highlight three points:

(1) astigmatic blur rapidly induces refractive astigmatism, reaching a peak by T2 (Fig. 1);
(2) crossed-cylindrical lens treatment leads to anterior chamber deepening and lens thinning as early as T2 (Fig. 4);
(3) the axis of imposed astigmatic blur (WTR vs. ATR) drives distinct compensatory responses (Figs. 1–3).

These results highlight the anterior segment's pivotal role in early-phase emmetropization under astigmatic blur, advancing our understanding of refractive plasticity mechanisms.

4.1. What drives rapid early refractive and corneal astigmatism development?

The rapid rise in refractive astigmatism (RA) by T1 and its stabilization by T2 (Fig. 1A) reveal an early sensitive window for astigmatism development. Crucially, RA peaked *before* corneal astigmatism (CA) (Fig. 2A), suggesting that initial compensation is driven primarily by internal optical mechanisms – particularly lenticular adjustments in its toricity (Fig. 3) – rather than corneal shape remodeling. Internal astigmatism (IA), defined as RA minus CA (Thibos et al., 1997), demonstrated compensatory behavior by exhibiting inverse patterns to CA (Figs. 2 and 3), consistent with human studies where internal optics offset corneal astigmatism (Huynh et al., 2006; Manny et al., 2016; Wang et al., 2019). However, since CA measurements began at T3, IA's critical role during the initial phase (T1-T2) remains inferred rather than directly measured. In our previous work (Chu and Kee, 2015), imposing a +4/−8 crossed-cylinder (zero mean spherical power) did not produce systematic changes in spherical equivalent versus controls, minimizing magnification or peripheral distortion concerns; likewise, comparing low- and high-magnitude cylindrical lenses of the same axis (+2/−4 vs + 4/−8 at 90° and 180°) showed no systematic differences in spherical equivalent or astigmatic axis and largely similar posterior shape metrics. In addition, refractive astigmatism rose robustly, correlated more strongly with internal than corneal astigmatism, and its principal component was specifically associated with meridional differences in posterior ocular expansion, indicating axis-specific compensation rather than generalized distortion. Refractive astigmatism also exceeded corneal astigmatism in most groups, supporting a dominant early role for internal optics with corneal shape remodeling following more slowly. These earlier findings from our laboratory therefore support that rapid compensation is triggered primarily by astigmatic blur.

The rapid response of RA aligns with studies demonstrating that optical defocus triggers choroidal changes within hours in animal models (Kee et al., 2001; Zhu et al., 2005) as well as human studies (Ostrin et al., 2023; Read et al., 2013). In the current study, we also observed choroidal thickening in WTR astigmatism at T1 (Fig. 4D), but choroidal thickness did not correlate directly with the steepest/flattest

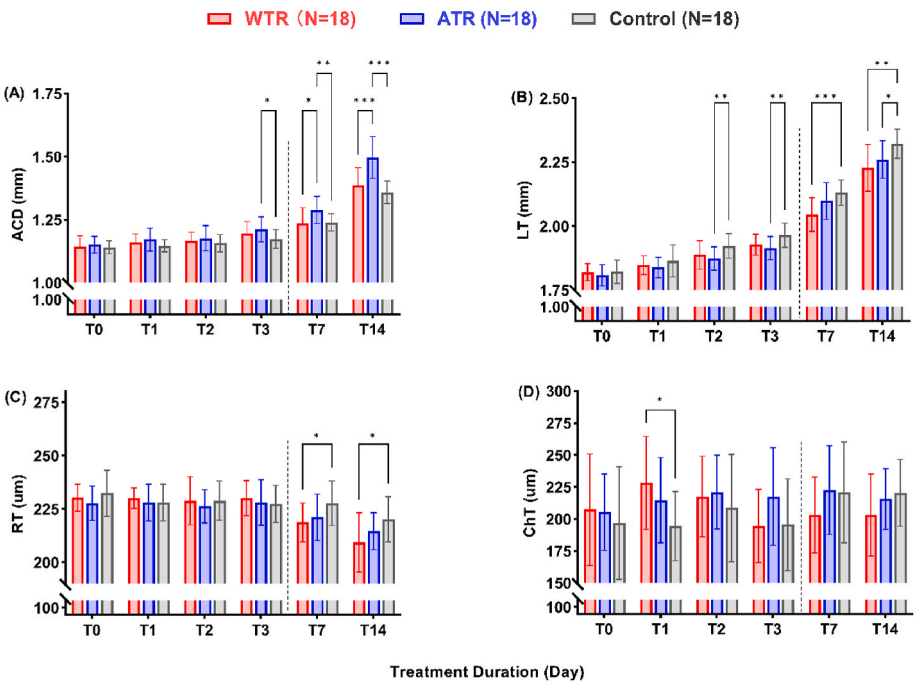

Fig. 4. Longitudinal changes in anterior chamber depth (**ACD**, A), lens thickness (**LT**, B), retinal thickness (**RT**, C), and choroidal thickness (**ChT**, D) for treated (WTR [red], ATR [blue]) and control [grey] groups. The vertical dashed line in the figures separates data into early and long-term phase exposure. Data: mean ± SD. Significance: *p < 0.05, **p < 0.01, ***p < 0.001. (For interpretation of the references to colour in this figure legend, the reader is referred to the Web version of this article.)

corneal meridians, suggesting that choroidal responses may operate independently of corneal curvature changes. Notably, the anterior ciliary muscle in chicks, known as Crampton's muscle, originates at the sclera with support from scleral ossicles and attaches to the corneal inner lamella (Glasser et al., 1994; Murphy et al., 1995), where its contraction alters corneal curvature by flattening the periphery and steepening the center through circumferential tension, thereby modulating corneal accommodation. Additionally, ciliary action is functionally linked with lens accommodation and may interact with choroidal changes, which are innervated via parasympathetic inputs associated with the ciliary region and influence both refractive compensation and ocular growth regulation (Rucker et al., 2023). Thus, ciliary muscle, lenticular adjustments, and choroidal remodeling may operate in an integrated manner, mediating refractive and structural compensation to imposed astigmatism in the developing eye.

4.2. Is anterior segment changes a compensatory mechanism for astigmatic blur?

The progressive anterior chamber deepening (ACD) and lens thinning (LT) in treated eyes (Fig. 4A and B) reveal a coordinated anterior segment response to astigmatic blur: ATR eyes exhibited earlier ACD increases and LT reductions than WTR/controls. This ACD-lens interplay mirrors findings in human myopia research: myopic eyes show deeper ACD than emmetropic and hyperopic eyes (Shih et al., 2009; Xiong et al., 2022), as well as faster myopic progression (>1.0 D over two years) correlated with greater ACD increases compared to slower progression (<1.0 D over two years) (Zhao et al., 2024). Furthermore, LT is thinner in myopic eyes than in emmetropes (Mutti et al., 2012; Rozema et al., 2019) and hyperopes (Lu et al., 2021).

Lens thinning emerged rapidly in ATR-treated eyes by day two and did not covary with the magnitude or axis of refractive, corneal, or internal astigmatism (data not shown), consistent with prior evidence that astigmatic blur does not evoke astigmatic accommodation in alert chicks (Thomas and Schaeffel, 2000) and with our measurements under isoflurane, which suppresses ciliary muscle activity. Together, these findings support accommodation-independent, visually guided remodeling of the lens. In light of the distinct accommodative mechanism in chicks—which likely involves ciliary muscle action on the lens annular pad via peripheral iris muscles (Glasser et al., 1995; Murphy et al., 1995; Choh & Sivak, 2005) (see contradictory finding from Ostrin et al., 2011)—the lens may respond differentially to specific visual cues and adjust its growth or microstructure via yet-undetermined signaling pathways. In terms of underlying mechanisms, lens thinning could arise from altered growth kinetics, hydration, or fiber organization; because the avian lens grows lifelong by adding concentric fiber cell layers without cell loss (Priolo et al., 1999), the potential role of fiber compaction in producing lens thinning remains to be established with high-resolution imaging and histology. We hypothesize that visual signals triggered by astigmatic blur engage a broader anterior segment response that includes lens-specific remodeling coordinated with corneal and choroidal changes. Future work will test these possibilities by quantifying lens microstructure and zonular/ciliary architecture and by examining their coupling to corneal and choroidal remodeling across the time course of astigmatism induction.

Anterior chamber deepening is hypothesized to compensate for lens thinning, maintaining a dynamic balance between axial length and refractive components (Zadnik et al., 2004). Myopia may develop when the crystalline lens fails to sufficiently reduce its optical power while the eyeball elongates rapidly (Han et al., 2024). Horizontal anterior lens flattening in elongated eyes (Chen et al., 2024) suggests structural lens plasticity needing further investigation. Future three-dimensional imaging (e.g., anterior segment OCT) could clarify whether lenticular morphology dynamically adapts to astigmatic blur, refining our understanding of the interplay between RA and CA.

Notably, in WTR eyes, both flattest and steepest corneal meridians showed negative correlations with VCD (Table 1), while in ATR eyes, only the steepest meridian correlated negatively at T14. This aligns with the chick study using sphero-cylindrical lenses to simulate hyperopic WTR/ATR astigmatic blurs (Vyas and Kee, 2021). These findings provide evidence for axis-specific anterior-posterior segment linkages, extending prior work primarily focusing on spherical defocus (Read

Table 1
The correlation between the corneal flattest/steepest meridian and individual ocular components in WTR/ATR group.

		CCT	ACD	VCD	RT	ChT
Kf (D)						
T3	WTR	–	***r* = –0.61, *p* = 0.008**	***r* = –0.86, *p* < 0.001**	–	–
	ATR	–	–	–	–	–
T7	WTR	–	–	***r* = –0.67, *p* = 0.002**	–	–
	ATR	r = −0.5, *p* = 0.035	–	–	–	–
T14	WTR	–	–	***r* = –0.73, *p* = 0.001**	r = 0.54, *p* = 0.022	r = 0.61, *p* = 0.008
	ATR	r = −0.51, *p* = 0.029	–	r = −0.69, *p* = 0.029	–	–
Ks (D)						
T3	WTR	–	r = −0.61, *p* = 0.007	***r* = –0.81, *p* < 0.001**	–	–
	ATR	–	–	r = −0.42, *p* = 0.028	–	–
T7	WTR	–	–	r = −0.61, *p* = 0.008	–	–
	ATR	r = −0.52, *p* = 0.028	–	–	–	–
T14	WTR	–	–	***r* = –0.79, *p* < 0.001**	r = 0.63, *p* = 0.005	r = 0.62, *p* = 0.006
	ATR	–	–	***r* = –0.67, *p* = 0.002**	–	–

The bolded and italic font shows the results remained statistical significance after Bonferroni correction (adjusted $p < 0.0024$). CCT: central corneal thickness; ACD: anterior chamber depth; VCD: vitreous chamber depth; RT: retinal thickness; ChT: choroidal thickness; Kf: flattest curvature; Ks: steepest curvature.

et al., 2010; Troilo et al., 2019) by demonstrating astigmatism-specific anterior-posterior segment interactions.

One potential pathway for such anterior segment influence involves signals originating from the peripheral retina. Specialized retinal ganglion cells, such as bullwhip and mini-bullwhip cells, are strategically distributed in the peripheral retina and have been implicated in controlling equatorial expansion and ocular shape modulation in chicks (Fischer et al., 2008). These cells may mediate the regulation of the corneal limbus growth during early developmental stages (Iribarren et al., 2012), linking peripheral retinal input directly with anterior segment remodeling. Therefore, astigmatic blur could disrupt refractive development by altering the signaling from the peripheral retina to anterior segment structures, leading to uncoordinated anterior changes that in turn perturb the coordinated growth of the entire globe.

4.3. Why WTR and ATR blur elicit different responses?

The decline in astigmatic components in the untreated controls (Figs. 2 and 3) reflects natural emmetropization ("sphericalization") during early postnatal growth, where corneal toricity decreases as the cornea becomes more spherical. This pattern is well documented in humans (Kee, 2013 & Read et al., 2014) and in animal models, including chick (Schmid and Wildsoet, 1997) and monkey (Kee et al., 2002). The longitudinal pattern of RA (Fig. 1), CA (Fig. 2) and IA (Fig. 3) among WTR- and ATR-treated chicks provided further evidence of eye's bidirectional adaptive and compensation systems (Chan et al., 2022; Chu and Kee, 2015; Hoseini-Yazdi et al., 2020; Liang et al., 2023, 2024; Vyas et al., 2022). When WTR astigmatism is imposed, the eye tends to develop compensatory ATR astigmatism, and vice versa. Consistent with previous chick studies, imposing WTR astigmatic blur induced higher magnitudes of astigmatism compared to ATR condition (Chu and Kee, 2015; Popa et al., 2020; Vyas and Kee, 2021). In addition, human studies also showed temporal compensation of astigmatism: exposure to WTR and ATR astigmatism using +3.00 D cylindrical lenses caused significant thickening following WTR blur and thinning after ATR blur in choroidal thickness (Hoseini-Yazdi et al., 2020), and J0 astigmatic component became less positive (from +1.53 DC to +1.28 DC) in the WTR condition and less negative (from −1.33 DC to −0.94 DC) in the ATR condition (Chan et al., 2022). These changes indicate an active process in the visual system aimed at minimizing the impact of astigmatic blur.

The observed difference in induced WTR versus ATR astigmatism magnitude may stem from anatomical, optical and physiological factors. Anatomically, greater vertical ocular compliance—potentially due to softer periocular tissues (extraocular muscles, connective tissue, and orbital fat)—could facilitate larger astigmatic changes in the WTR group, where vertical meridian expansion exceeds horizontal constraints (i.e., a flatter vertical meridian) (Atchison et al., 2004). Optically, WTR astigmatism demonstrates better visual tolerance in some studies, with lens-induced WTR causing less acuity reduction than ATR astigmatism (Hughes et al., 2017; Ohlendorf et al., 2011; Serra et al., 2018) (though conflicting evidence exists (Liang et al., 2023; Singh et al., 2013)). This is supported by contrast sensitivity adaptations showing 33 % improvement for WTR versus 26 % for ATR across spatial frequencies, indicating stronger neural compensation for WTR blur (Leung et al., 2023). Clinically, WTR astigmatism is consistently reported as more adaptable in corrective lens wear. Collectively, these factors suggest that superior physiological tolerance to WTR astigmatism may enable a sustained compensatory response, gradually increasing ATR astigmatism to optimize optical clarity.

4.4. Implications for refractive development

Using chick model, we revealed anterior dominance in astigmatism compensation, suggesting that astigmatic blur may interfere with refractive development through distinct mechanisms. Notably, in this study, despite significant changes in anterior chamber depth and lens thickness (Fig. 4), axial length remained largely unchanged, implying that eye growth regulation in response to astigmatic blur involves distinct yet integrated regulatory networks encompassing both anterior and posterior segments. Regardless of how astigmatic blur affects the anterior segment, previous studies have demonstrated that different types of astigmatic blur influence ocular growth differently. For example, imposing hyperopic-ATR blur in chicks induced more myopia than hyperopic-WTR blur (Vyas and Kee, 2021), and children with baseline ATR astigmatism exhibited faster axial elongation compared to those with initial WTR astigmatism (Liang et al., 2024).

Emerging clinical studies reported increased astigmatism in children using specially designed lenses for myopia control (Wang et al., 2025; Xu

et al., 2025). Although these lenses effectively slow axial elongation and myopia progression, a subset of children develop new or persistent astigmatism during treatment, which may confound the myopia-control effect. Moreover, one study found that baseline astigmatism can reduce the efficacy of myopia-control interventions and that younger children or those with higher initial astigmatism may have less favorable refractive outcomes (Domsa et al., 2024). Taken together with findings from the chick model, these results suggest that clinicians should pay closer attention to the anterior segment in children with higher astigmatism.

4.5. Limitations

This study shows characterization of ocular component dynamics during two weeks of crossed-cylindrical lens treatment using a relatively large sample of chickens, providing foundational insights into astigmatism-driven adaptations. However, several limitations warrant consideration. First, axial ocular measurements, while informative of overall eyeball change, do not reflect spatial changes in shape. We acknowledge that isoflurane can influence intraocular pressure and ocular biometry; in guinea pigs, 10–20 min of anesthesia (5 % in 1.5 L/min O2) increased lens thickness by 0.4–0.6 % and decreased anterior chamber depth by 4.4–6.1 % (Myles et al., 2024). In contrast, our chick data show the opposite pattern—early and persistent lens thinning and anterior chamber deepening under astigmatic blur—with biometric measurements obtained within a short, consistent window (~3 min per bird), using an identical, standardized protocol and a single trained investigator (LY) across all conditions. Our analyses emphasize comparisons across treatment conditions rather than absolute values, further minimizing systematic bias from anesthesia. While we cannot exclude a small contribution of isoflurane, the directionality, timing, and condition-specific patterns observed here argue that the reported anesthetic effects cannot account for the primary findings. We also note that isoflurane likely reduced accommodative fluctuations, increasing the consistency of biometry across groups. Second, because internal astigmatism was computed rather than directly measured, the role of internal optics (e.g., crystalline lens toricity and morphology) remains undercharacterized; integrating three-dimensional live imaging (such as anterior segment OCT or MRI) in future work will allow direct quantification of lens changes and their interplay with corneal remodeling during astigmatism development. Third, corneal shape measurement began at T3, as earlier time points (T0-T2) lacked sufficient corneal size for reliable topography, limiting the ability to early assessment of corneal changes. Future studies can employ more sensitive and adaptable imaging technologies, such as high-resolution AS-OCT or Scheimpflug imaging, which can provide detailed anterior and posterior corneal curvature mapping even in small or rapidly developing eyes. Finally, while the chick model cannot replicate human physiology in full—differences include a faster developmental timeline, species-specific accommodation mechanics that involve the cornea in chicks, and distinct anterior segment biomechanics—it offers key advantages for isolating causal effects of astigmatic blur that are not feasible in humans. In chicks, axis-specific astigmatic blur can be precisely induced and controlled, anterior segment changes can be measured frequently across early development, and tissue-level assessments can be performed without the ethical and practical constraints of pediatric studies. Importantly, the chick cornea shares relevant anatomical features with the human cornea, including a true Bowman's membrane (absent in rabbits and rodents) and similar relative layer thickness ratios despite being overall thinner (Fowler et al., 2004; Wisely et al., 2017; Ritchey et al., 2011). These similarities support cautious translational interpretation, while the model's experimental control strengthens causal inference about how astigmatic blur drives anterior segment remodeling. Taken together, these advancements would clarify whether astigmatism-induced signals propagate axis-specific adjustments across ocular compartments, as suggested by differential RA-VCD correlations in WTR/ATR groups. By bridging spatial, morphological, and temporal gaps, future work could elucidate how localized blur gradients orchestrate coordinated anterior-posterior segment adaptations, refining models of refractive error pathogenesis.

5. Conclusion

This study establishes astigmatic blur as a potent driver of anterior segment structural remodeling, with rapid corneal and lenticular changes (i.e. lens thinning) modulating refractive development within days. The axis-specific responses and early-phase dynamics provide critical insights for optimizing clinical interventions in astigmatism-prone populations. Future work should explore molecular pathways linking corneal shape remodeling to lenticular changes, leveraging this model to dissect the spatiotemporal hierarchy of astigmatism compensation mechanisms.

CRediT authorship contribution statement

Yuanyuan Liang: Writing – review & editing, Writing – original draft, Visualization, Project administration, Methodology, Investigation, Formal analysis, Data curation, Conceptualization. **Tsz Wing Leung:** Writing – review & editing, Visualization. **Patience Ansomah Ayerakwah:** Writing – review & editing. **Byung Soo Kang:** Writing – review & editing. **Chea-su Kee:** Writing – review & editing, Writing – original draft, Supervision, Resources, Methodology, Investigation, Funding acquisition, Formal analysis, Data curation.

Funding

This study was supported by the Innovation and Technology Commission of the HKSAR Government (ITC InnoHK CEVR Project 1.5)

Conflict of interest

The authors declare the following financial interests/personal relationships which may be considered as potential competing interests: Kee Chea su reports financial support was provided by Innovation and Technology Commission of the HKSAR Government (ITC InnoHK CEVR Project 1.5). If there are other authors, they declare that they have no known competing financial interests or personal relationships that could have appeared to influence the work reported in this paper.

Acknowledgements

The authors genuinely thank anonymous reviewers for providing constructive and helpful comments.

Appendix A. Supplementary data

Supplementary data to this article can be found online at https://doi.org/10.1016/j.exer.2026.110861.

Data availability

Data will be made available on request.

References

Ashby, R.S., Schaeffel, F., 2010. The effect of bright light on lens compensation in chicks. Investig. Ophthalmol. Vis. Sci. 51, 5247–5253.

Atchison, D.A., Jones, C.E., Schmid, K.L., Pritchard, N., Pope, J.M., Strugnell, W.E., Riley, R.A., 2004. Eye shape in emmetropia and myopia. Investig. Ophthalmol. Vis. Sci. 45, 3380–3386.

Ayerakwah, P.A., Kang, B.S., Liang, Y., Chan, H.H.L., Kee, C.S., Leung, T.W., 2025. Astigmatic blur in partial visual field exposure induces astigmatism compensation in developing chick eyes. Investig. Ophthalmol. Vis. Sci. 66, 43-43.

Black, A.A., Wood, J.M., Colorado, L.H., Collins, M.J., 2019. The impact of uncorrected astigmatism on night driving performance. Ophthalmic Physiol. Opt. 39, 350–357.
Chan, K.H., Shik, H.T., Kwok, K.W., Kee, C.S., Leung, T.W., 2022. Bi-directional refractive compensation for with-the-rule and against-the-rule astigmatism in young adults. Investig. Ophthalmol. Vis. Sci. 63, 15-15.
Chen, C., Meng, J., Cheng, K., Kang, C., Zhou, L., Guo, H., Zhu, X., 2024. Spatial and morphologic features of lenses with different axial lengths in cataract patients: a swept-source optical coherence tomography-based study. BMC Ophthalmol. 24, 542.
Choh, V., Sivak, J.G., 2005. Lenticular accommodation in relation to ametropia: the chick model. J. Vis. 5, 2- 2.
Chu, G.C.H., Zhou, Y., Zheng, Y., Kee, C.S., 2014. Bi-directional corneal accommodation in alert chicks with experimentally-induced astigmatism. Vis. Res. 98, 26–34.
Chu, G.C.H., Kee, C.S., 2015. Effects of optically imposed astigmatism on early eye growth in chicks. PLoS One 10, e0117729.
COMET-Group, 2013. Myopia stabilization and associated factors among participants in the correction of myopia evaluation trial (COMET). Investig. Ophthalmol. Vis. Sci. 54, 7871.
Domsa, P., Bankó, É.M., Körtvélyes, J., Meigen, C., Széchey, R., Lantos, K., Nagy, Z.Z., Csutak, A., 2024. Astigmatism and maternal myopia as important factors affecting success rate of DIMS lens treatment. BMJ Open Ophthalmol 9.
Fischer, A.J., Ritchey, E.R., Scott, M.A., Wynne, A., 2008. Bullwhip neurons in the retina regulate the size and shape of the eye. Devel Biol 317, 196–212.
Fowler, W.C., Chang, D.H., Roberts, B.C., Zarovnaya, E.L., Proia, A.D., 2004. A new paradigm for corneal wound healing research: the white leghorn chicken (Gallus gallus domesticus). Curr. Eye Res. 28, 241–250.
Glasser, A., Troilo, D., Howland, H.C., 1994. The mechanism of corneal accommodation in chicks. Vis. Res. 34, 1549–1566.
Glasser, A., Murphy, C.J., Troilo, D., Howland, H.C., 1995. The mechanism of lenticular accommodation in chicks. Vis. Res. 35, 1525–1540.
Gottlieb, M.D., Fugate-Wentzek, L.A., Wallman, J., 1987. Different visual deprivations produce different ametropias and different eye shapes. Investig. Ophthalmol. Vis. Sci. 28, 1225–1235.
Han, X., Xiong, R., Jin, L., Chang, S., Chen, Q., Wang, D., Chen, X., Qu, Y., Liu, W., He, M., 2024. Role of lens in early refractive development: evidence from a large cohort of Chinese children. Br. J. Ophthalmol. 108, 1627–1633.
Hashemi, H., Fotouhi, A., Yekta, A., Pakzad, R., Ostadimoghaddam, H., Khabazkhoob, M., 2018. Global and regional estimates of prevalence of refractive errors: systematic review and meta-analysis. J Curr Ophthalmol 30, 3–22.
Hoseini-Yazdi, H., Vincent, S.J., Read, S.A., Collins, M.J., 2020. Astigmatic defocus leads to short-term changes in human choroidal thickness. Investig. Ophthalmol. Vis. Sci. 61, 48-48.
Hughes, A.R., Mallen, E.A., Elliott, D.B., 2017. The visual impact of lens-induced astigmatism is linked to habitual axis. Optom. Vis. Sci. 94, 260–264.
Huynh, S.C., Kifley, A., Rose, K.A., Morgan, I., Heller, G.Z., Mitchell, P., 2006. Astigmatism and its components in 6-year-old children. Investig. Ophthalmol. Vis. Sci. 47, 55–64.
Iribarren, R., Bonthoux, F.F., Pfortner, T., Chiaradia, P., Stell, W.K., 2012. Corneal power is correlated with anterior chamber diameter. Investig. Ophthalmol. Vis. Sci. 53, 3788–3791.
Irving, E., Callender, M., Sivak, J., 1991. Inducing myopia, hyperopia, and astigmatism in chicks. Optom. Vis. Sci. 68, 364–368.
Irving, E., Callender, M., Sivak, J., 1995. Inducing ametropias in hatchling chicks by defocus—aperture effects and cylindrical lenses. Vis. Res. 35, 1165–1174.
Kang, B.S., Leung, T.W., Vyas, S.A., Ayerakwah, P.A., Lin, J., Liang, Y., Stell, W.K., Kee, C.S., 2024. Synchronous myopia development induced by bilateral form deprivation in chicks. Exp. Eye Res. 239, 109783.
Kang, B.S., Wang, L.K., Zheng, Y.P., Guggenheim, J.A., Stell, W.K., Kee, C.S., 2018. High myopia induced by form deprivation is associated with altered corneal biomechanical properties in chicks. PLoS One 13, e0207189.
Kearney, S., Shah, R., Vlasak, N., 2025. The role of astigmatism in myopia development, myopia progression and myopia control. Ophthalmic Physiol. Opt. 45, 1946–1964.
Kee, C.S., Hung, L.F., Qiao, Y., Habib, A., Smith, E.L., 2002. Prevalence of astigmatism in infant monkeys. Vis. Res. 42, 1349–1359.
Kee, C.S., 2013. Astigmatism and its role in emmetropization. Exp. Eye Res. 114, 89–95.
Kee, C.S., Deng, L., 2008. Astigmatism associated with experimentally induced myopia or hyperopia in chickens. Investig. Ophthalmol. Vis. Sci. 49, 858–867.
Kee, C.S., Marzani, D., Wallman, J., 2001. Differences in time course and visual requirements of ocular responses to lenses and diffusers. Investig. Ophthalmol. Vis. Sci. 42, 575–583.
Leung, T.W., Li, R.W., Kee, C.S., 2021. Meridional anisotropy of foveal and peripheral resolution acuity in adults with emmetropia, myopia, and astigmatism. Investig. Ophthalmol. Vis. Sci. 62, 11-11.
Leung, T.W., Li, R.W., Kee, C.S., 2023. Brief adaptation to astigmatism reduces meridional anisotropy in contrast sensitivity. Investig. Ophthalmol. Vis. Sci. 64, 4-4.
Liang, D., Du, B., Leung, T.W., Liu, Z., Su, Q., Jin, N., Zhang, Z., He, M., Yan, H., Wei, R., 2024. Impact of astigmatism on axial elongation in school-age children: a five-year population-based study in tianjin, China. Investig. Ophthalmol. Vis. Sci. 65, 45-45.
Liang, D., Leung, T.W., Kee, C.S., 2023. Measuring retinal thickness and visual acuity in eyes with different types of astigmatism in a cohort of Hong Kong Chinese adults. Investig. Ophthalmol. Vis. Sci. 64, 2-2.
Lu, T., Song, J., Wu, Q., Jiang, W., Tian, Q., Zhang, X., Xu, J., Wu, J., Hu, Y., Sun, W., 2021. Refractive lens power and lens thickness in children (6–16 years old). Sci. Rep. 11, 19284.
Manny, R.E., Deng, L., Gwiazda, J., Hyman, L., Weissberg, E., Scheiman, M., Fern, K.D., 2016. Internal astigmatism in myopes and non-myopes: compensation or constant? Optom. Vis. Sci. 93, 1079.
Myles, W.E., Abdulla, Y., McFadden, S.A., 2024. Effect of isoflurane anaesthetic time on ocular a-scan ultrasonography measures and their relationship to age and OCT measures in the Guinea pig. Exp. Eye Res. 243, 109914.
Mitchell, D.E., Freeman, R.D., Millodot, M., Haegerstrom, G., 1973. Meridional amblyopia: evidence for modification of the human visual system by early visual experience. Vis. Res. 13, 535. I.
Murphy, C.J., Glasser, A., Howland, H.C., 1995. The anatomy of the ciliary region of the chicken eye. Investig. Ophthalmol. Vis. Sci. 36, 889–896.
Mutti, D.O., Mitchell, G.L., Sinnott, L.T., Jones-Jordan, L.A., Moeschberger, M.L., Cotter, S.A., Kleinstein, R.N., Manny, R.E., Twelker, J.D., Zadnik, K., 2012. Corneal and crystalline lens dimensions before and after myopia onset. Optom. Vis. Sci. 89, 251–262.
Nickla, D.L., Wildsoet, C., Wallman, J., 1998. Visual influences on diurnal rhythms in ocular length and choroidal thickness in chick eyes. Exp. Eye Res. 66, 163–181.
Ohlendorf, A., Tabernero, J., Schaeffel, F., 2011. Visual acuity with simulated and real astigmatic defocus. Optom. Vis. Sci. 88, 562–569.
Ostrin, L.A., Liu, Y., Choh, V., Wildsoet, C.F., 2011. The role of the iris in chick accommodation. Investig. Ophthalmol. Vis. Sci. 52, 4710–4716.
Ostrin, L.A., Harb, E., Nickla, D.L., Read, S.A., Alonso-Caneiro, D., Schroedl, F., Kaser-Eichberger, A., Zhou, X., Wildsoet, C.F., 2023. IMI—The dynamic choroid: new insights, challenges, and potential significance for human myopia. Investig. Ophthalmol. Vis. Sci. 64, 4-4.
Popa, A.-V., Kee, C.S., Stell, W.K., 2020. Retinal control of lens-induced astigmatism in chicks. Exp. Eye Res., 108000
Priolo, S., Sivak, J., Kuszak, J., 1999. Effect of age on the morphology and optical quality of the avian crystalline lens. Exp. Eye Res. 69, 629–640.
Qin, Z., Peng, T., Zhang, Z., Lou, J., Wang, C., Deng, R., Xu, M., Yu, X., Chen, W., 2022. Myopia progression and stabilization in school-aged children with single-vision lenses. Acta Ophthalmol. 100, e950–e956.
Read, S.A., Collins, M.J., Carney, L.G., 2007. A review of astigmatism and its possible genesis. Clin. Exp. Optom. 5–19.
Read, S.A., Collins, M.J., Sander, B.P., 2010. Human optical axial length and defocus. Investig. Ophthalmol. Vis. Sci. 51, 6262–6269.
Read, S.A., Collins, M.J., Vincent, S.J., Alonso-Caneiro, D., 2013. Choroidal thickness in myopic and nonmyopic children assessed with enhanced depth imaging optical coherence tomography. Investig. Ophthalmol. Vis. Sci. 54, 7578–7586.
Read, S.A., Vincent, S.J., Collins, M.J., 2014. The visual and functional impacts of astigmatism and its clinical management. Ophthalmic Physiol. Opt. 34, 267–294.
Ritchey, E.R., Code, K., Zelinka, C.P., Scott, M.A., Fischer, A.J., 2011. The chicken cornea as a model of wound healing and neuronal re-innervation. Mol. Vis. 17, 2440.
Rozema, J., Dankert, S., Iribarren, R., Lanca, C., Saw, S.-M., 2019. Axial growth and lens power loss at myopia onset in Singaporean children. Investig. Ophthalmol. Vis. Sci. 60, 3091–3099.
Rucker, F., Taylor, C., Kaser-Eichberger, A., Schroedl, F., 2023. Parasympathetic and sympathetic control of emmetropization in chick. Exp. Eye Res. 232, 109508.
Schmid, K.L., Wildsoet, C.F., 1997. Natural and imposed astigmatism and their relation to emmetropization in the chick. Exp. Eye Res. 64, 837–847.
Serra, P.M., Cox, M.J., Chisholm, C.M., 2018. The effect of astigmatic axis on visual acuity measured with different alphabets in Roman alphabet readers. Clin. Optom. 93–102.
Shih, Y.F., Chiang, T.H., Lin, L.L.K., 2009. Lens thickness changes among schoolchildren in Taiwan. Investig. Ophthalmol. Vis. Sci. 50, 2637–2644.
Singh, A., Pesala, V., Garg, P., Bharadwaj, S.R., 2013. Relation between uncorrected astigmatism and visual acuity in pseudophakia. Optom. Vis. Sci. 90, 378–384.
Thibos, L.N., Wheeler, W., Horner, D., 1997. Power vectors: an application of Fourier analysis to the description and statistical analysis of refractive error. Optom. Vis. Sci. 74, 367–375.
Thomas, S., Schaeffel, F., 2000. Developmental compensation of imposed astigmatism is not initiated by astigmatic accommodation in chickens. Vis. Res. 40, 3553–3558.
Troilo, D., Li, T., Glasser, A., Howland, H.C., 1995. Differences in eye growth and the response to visual deprivation in different strains of chicken. Vis. Res. 35, 1211–1216.
Troilo, D., Smith, E.L., Nickla, D.L., Ashby, R., Tkatchenko, A.V., Ostrin, L.A., Gawne, T. J., Pardue, M.T., Summers, J.A., Kee, C.S., 2019. IMI–report on experimental models of emmetropization and myopia. Investig. Ophthalmol. Vis. Sci. 60, M31–M88.
Vyas, S.A., Kee, C.S., 2021. Early astigmatism can alter myopia development in chickens. Investig. Ophthalmol. Vis. Sci. 62, 27-27.
Vyas, S.A., Lakshmanan, Y., Chan, H.H.l., Leung, T.W., Kee, C.S., 2022. Experimentally induced myopia and myopic astigmatism alter retinal electrophysiology in chickens. Sci. Rep. 12, 21180.
Wallman, J., Wildsoet, C., Xu, A., Gottlieb, M.D., Nickla, D.L., Marran, L., Krebs, W., Christensen, A.M., 1995. Moving the retina: choroidal modulation of refractive state. Vis. Res. 35, 37–50.
Wallman, J., Winawer, J., 2004. Homeostasis of eye growth and the question of myopia. Neuron 447–468.
Wang, L., Zhang, Q., Zhou, T., Yu, W., Wang, J., Li, R., Chen, Q., Que, Q., Gao, X., 2025. Association between myopia progression and cylinder power progression in defocus incorporated multiple segments lens wearers. Sci. Rep. 15, 24143.
Wang, L.L., Wang, W., Han, X.T., He, M.G., 2018. Influence of severity and types of astigmatism on visual acuity in school-aged children in southern China. Int. J. Ophthalmol. 11, 1377–1383.
Wang, Z., Huang, D., Chen, X., Zhu, H., Sun, Q., Wang, Y., Zhang, X., Zhai, L., Wang, C., Liu, H., 2019. Preschool children exhibit evident compensatory role of internal astigmatism in distribution of astigmatism: the nanjing eye study. Investig. Ophthalmol. Vis. Sci. 60, 73–81.

Wisely, C.E., Sayed, J.A., Tamez, H., Zelinka, C., Abdel-Rahman, M.H., Fischer, A.J., Cebulla, C.M., 2017. The chick eye in vision research: an excellent model for the study of ocular disease. Prog. Retin. Eye Res. 61, 72–97.
Wolffsohn, J.S., Bhogal, G., Shah, S., 2011. Effect of uncorrected astigmatism on vision. J. Cataract Refract. Surg. 37, 454–460.
Xiong, S., He, X., Sankaridurg, P., Zhu, J., Wang, J., Zhang, B., Zou, H., Xu, X., 2022. Accelerated loss of crystalline lens power initiating from emmetropia among young school children: a 2-year longitudinal study. Acta Ophthalmol. 100, e968–e976.
Xu, W., Li, X., Zhang, J., Li, H., Ding, X., Hu, X., Quan, X., Su, Y., Lu, F., Chen, J., 2025. The peripheral defocus designed spectacle lenses might increase astigmatism in myopic children. Transl. Vis. Sci. Technol. 14, 8-8.
Zadnik, K., Mutti, D.O., Mitchell, G.L., Jones, L.A., Burr, D., Moeschberger, M.L., 2004. Normal eye growth in emmetropic schoolchildren. Optom. Vis. Sci. 81, 819–828.
Zhang, J., Wu, Y., Sharma, B., Gupta, R., Jawla, S., Bullimore, M.A., 2023. Epidemiology and burden of astigmatism: a systematic literature review. Optom. Vis. Sci. 100, 218–231.
Zhao, Y., Ye, Y., Geng, J., Zhang, J., Zhang, Z., Xian, Y., Huang, Y., Liu, F., Xu, Y., Zhou, X., 2024. Differences in anterior ocular biometric characteristics among 6-year-old children with different myopic shift rates: a 2-year longitudinal study. Asia-Pac J Ophthalmol 13, 100116.
Zhu, X., Park, T.W., Winawer, J., Wallman, J., 2005. In a matter of minutes, the eye can know which way to grow. Investig. Ophthalmol. Vis. Sci. 46, 2238–2241.
Zhu, X., Wallman, J., 2009. Temporal properties of compensation for positive and negative spectacle lenses in chicks. Investig. Ophthalmol. Vis. Sci. 50, 37–46.
Zhang, X.J., Wong, P.P.Y., Wong, E.S., Kam, K.W., Yip, B.H.K., Zhang, Y., Zhang, W., Young, A.L., Chen, L.J., Ip, P., 2022. Delayed diagnosis of amblyopia in children of lower socioeconomic families: the Hong Kong children eye study. Ophthalmic Epidemiol. 29, 621–628.